Chinese Physics C

Ultra-high order harmonic generation via a free electron laser mechanism[*]

DENG Hai-Xiao(邓海啸)[1)]　　DAI Zhi-Min(戴志敏)

Shanghai Institute of Applied Physics, Chinese Academy of Sciences, Shanghai 201800, China

Abstract　In this paper, by using the "frequency up-conversion" principle with a high gain harmonic generation free electron laser and an external seed laser, we consider the possibility of modulating a relativistic electron beam on the attosecond scale, so that it can produce coherent spontaneous radiation from the deep ultraviolet to the hard X-ray spectral region with a very short radiator. Analytical estimation and three-dimensional numerical modeling show the great potential to reach ultra-high harmonics up to several thousand. For an electron bunch with the typical quality as in the free electron laser scheme and a seed laser with 800 nm wavelength, 0.8 nm attosecond trains with alterable duration and GW scale peak power are modeled. The output radiation exhibits good shot-to-shot stability, full coherence and perfect tuning ability between the discrete harmonics of the seed frequency.

Key words　FEL, harmonic, attosecond, coherent

PACS　41.60.Cr, 42.65.Ky, 41.60.-m

1　Introduction

The availability of short wavelength radiation is of great interest in the free electron laser (FEL) community. One of the most feasible ways for delivering FEL to the hard X-ray is self amplified spontaneous emission (SASE) [1, 2]. However, SASE radiation starts from shot noise of the electron beam, and results in a poor temporal coherence and a long undulator system. With the growing interest in compact and fully temporal coherent sources, various seeded FEL schemes [3–5] have been proposed for short wavelengths on the basis of harmonic generation and seeding of external lasers. A typical scheme is high gain harmonic generation (HGHG), which has been demonstrated in the visible and ultraviolet region [6, 7]. Since HGHG pursues the exponential growth in the long radiator, it suffers from a limited frequency multiplication factor to avoid large beam energy modulation [8]. Recently, modifications to the standard HGHG have been proposed to improve the efficiency of frequency up-conversion [9–11]. However, the essential obstacle has not been overcome and the harmonic number is still in the range of 10 to 30.

In parallel, high brightness electron beam development has been dramatically driven by FEL applications in the last decade. A state-of-the-art photocathode gun can generate electron beams with a local energy spread of less than 6 keV and normalized emittance of 1 µm·rad [12]. Even when the effects on the energy spread induced by further acceleration, the bunch compression and laser heater [13, 14] are taken into account, the relative sliced energy spread of the electron beam can still be 10^{-5} level at the entrance of an X-ray FEL undulator. Moreover, the electron beam quality can be significantly enhanced in low charge operation, which is now considered by many FEL projects [15, 16].

In this paper, by using a state-of-the-art electron beam, the ultra-high order harmonic generation of intense laser via FEL mechanism is investigated. The harmonic generation scheme used the same basic elements as in the standard HGHG, but the key aspect is that the period number of the radiator in this discussion is much less than the harmonic up-conversion number. Thus, no exponential growth is expected in the radiator and large energy modulation

in the modulator is acceptable. Under such circumstances, the radiator radiation is highly relevant with the local micro-structure of the electron beam over one seed laser wavelength. However, the local micro-structure over one seed laser wavelength is averaged and smeared in the existing analytical and numerical model. Thus, appropriate analytical estimates and a three-dimensional numerical model are developed to investigate the ultra-high order harmonic generation in the quasi-HGHG scheme. Studies indicate great potential of reaching ultra-high harmonic generations up to several thousand, and the output radiation shows good stability, plus transverse and longitudinal coherence. As we shall explain in the following, one by product is the generation of attosecond X-ray trains, which is another important goal of the FEL community [17–20].

2 Density modulation of the electron beam

The ultra-high order harmonic generation scheme of using two-stage undulators and an external seed laser is shown in Fig. 1. A seed laser with wavelength λ_s interacts with a relativistic electron beam with average energy $\gamma_0 mc^2$ in the modulator with the resonant wavelength tuned to λ_s. Generally, the pulse length of the electron beam is much larger than the laser wavelength, and the beam current variation over the distance of several laser wavelengths can be neglected. Thus, the longitudinal distribution of the initial beam can be written as Eq. (1),

$$f(\gamma,\theta) = \frac{1}{\sqrt{2\pi}\sigma_\gamma} \; e^{-\frac{(\gamma-\gamma_0)^2}{2\sigma_\gamma^2}}, \tag{1}$$

where σ_γ is the rms energy spread of the electron beam. After passing through the modulator, the beam energy is modulated to (γ', θ')

$$\begin{aligned} \gamma' &= \gamma + \Delta\gamma\sin\theta \\ \theta' &= \theta \end{aligned}, \tag{2}$$
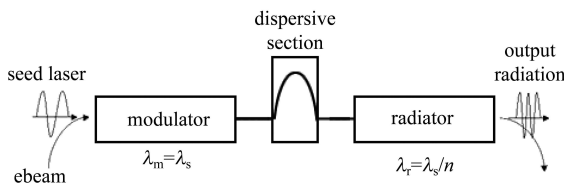

Fig. 1. Ultra-high order harmonic generation scheme using two undulators and an external seed laser.

where $\Delta\gamma$ is the maximum energy modulation at the end of the modulator, which can be calculated from the modulator length and the seed laser power. The dispersive section changes the energy modulation to density modulation. In a radiator resonant at wavelength of λ_s/n, the longitudinal rotations are given by the new coordinate (γ'', θ''),

$$\begin{aligned} \gamma'' &= \gamma' \\ \theta'' &= \theta' + \frac{\partial\theta}{\partial\gamma}(\gamma'-\gamma_0) \end{aligned}, \tag{3}$$

with the total dispersive strength $\partial\theta/\partial\gamma$ contributed from the modulator, the dispersive section and the radiator:

$$\frac{\partial\theta}{\partial\gamma} = \frac{4\pi}{\gamma_0}\left(\frac{N_1}{2} + N_d + \frac{N_2}{n}\right). \tag{4}$$

Here, the first and third terms are the dispersions in the modulator and the radiator, respectively, with N_1 and N_2 the undulator periods passed by the electron bunch. The harmonic number n is present in the third term because the electron phase in the radiator is n times that of the modulator. Since the energy modulation approximately increases linearly with the modulator length, the phase advance, obtained by integration, contributes a factor $1/2$ to cancel the factor 2 in the FEL phase equation when compared with the other two terms [14]. N_d is the equivalent strength of dispersive section [21], and $N_d = 0$ is assumed all through the discussion for simplicity. The longitudinal distribution function is shown in Eq. (5):

$$f(\gamma'',\theta'') = \frac{1}{\sqrt{2\pi}\sigma_\gamma} e^{-\frac{\left[\gamma''-\Delta\gamma\sin\left(\theta''-\frac{\partial\theta}{\partial\gamma}\gamma''\right)\right]^2}{2\sigma_\gamma^2}}. \tag{5}$$

Integration of f over γ'' expresses the longitudinal distribution of the beam density:

$$f(\theta'') = \int_{-\infty}^{\infty} f(\gamma'',\theta'')d\gamma'' = 1 +$$
$$2\sum_{m=1}^{\infty} e^{-(m\frac{\partial\theta}{\partial\gamma}\sigma_\gamma)^2/2} J_m\left[-m\frac{\partial\theta}{\partial\gamma}\Delta\gamma\right]\cos m\theta''. \tag{6}$$

FEL radiation is highly relevant to the longitudinal distribution of the electron beam, especially the beam current and the bunching parameter. After the modulator, the attosecond scale micro-structures come out over one seed wavelength [22], instead of the original uniform distribution. Moreover, the electrons in $[0, 2\pi]$ in the modulator are transformed to $[0, 2n\pi]$ in the radiator, and the bunching parameter corresponding to λ_s/n in the radiator is no more uniform over the distance of λ_s. Thus, we uniformly

divide the electrons over the distance λ_s into n slices and define the local current factor I and the local bunching factor B as follows:

$$I_n(\theta_0, N_2) = \frac{\displaystyle\int_{\theta_0-\pi/n}^{\theta_0+\pi/n} f(N_2, \theta'') \mathrm{d}\theta''}{2\pi/n}, \qquad (7)$$

$$B_n(\theta_0, N_2) = \frac{\displaystyle\int_{\theta_0-\pi/n}^{\theta_0+\pi/n} f(N_2, \theta'') \mathrm{e}^{-\mathrm{i}n\theta''} \mathrm{d}\theta''}{\displaystyle\int_{\theta_0-\pi/n}^{\theta_0+\pi/n} f(N_2, \theta'') \mathrm{d}\theta''}, \qquad (8)$$

where λ_s/n is the longitudinal length and θ_0 is the centre of each slice. After some brief calculations, one obtains

$$I_n(\theta_0, N_2) = 1 + \frac{2n}{\pi}\sum_{m=1}^{\infty} p_m b_m, \qquad (9)$$

$$B_n(\theta_0, N_2) = \frac{\displaystyle\sum_{m=1}^{\infty} q_m b_m}{\dfrac{\pi}{n} + 2\displaystyle\sum_{m=1}^{\infty} p_m b_m}, \qquad (10)$$

with

$$p_m = \frac{\cos m\theta_0 \sin\dfrac{m}{n}\pi}{m},$$

$$q_m = \frac{\mathrm{e}^{\mathrm{i}(m-n)\theta_0}\sin\dfrac{m-n}{n}\pi}{m-n} + \frac{\mathrm{e}^{-\mathrm{i}(m+n)\theta_0}\sin\dfrac{m+n}{n}\pi}{m+n},$$

$$b_m = \mathrm{e}^{-(m\frac{\partial\theta}{\partial\gamma}\sigma_\gamma)^2/2} J_m\left[-m\frac{\partial\theta}{\partial\gamma}\Delta\gamma\right].$$

For a harmonic generation scheme with low n, just as an HGHG, when the radiator radiation slips forward, the electron beam over the distance λ_s, the longitudinal beam distribution varies slightly. Thus, the local current factor and local bunching factor can be averaged over λ_s. Then Eqs. (9) and (10) will reduce to the universal results reported in Refs. [14, 21].

3 Ultra-high order harmonic generation

For ultra-high order harmonics, Bessel function $J_m(mx)$ has the maximum at $x \approx 1$. When appropriate parameters are chosen for the modulator and the seed laser, strong coherent ultra-high order harmonics are expected in the radiator. With a group of optimized parameters (as seen in Table 1), Fig. 2 shows an example with the frequency up-conversion factor $n = 1000$. When strong energy modulation $\Delta\gamma = 62.5$ is induced at the modulator exit, many electrons are modulated to the position around $\theta_0 = \pi$, where

the local beam current is enhanced to 103 times the initial uniform current and the local bunching factor remains 0.32. This indicates significant harmonic generation in the radiator.
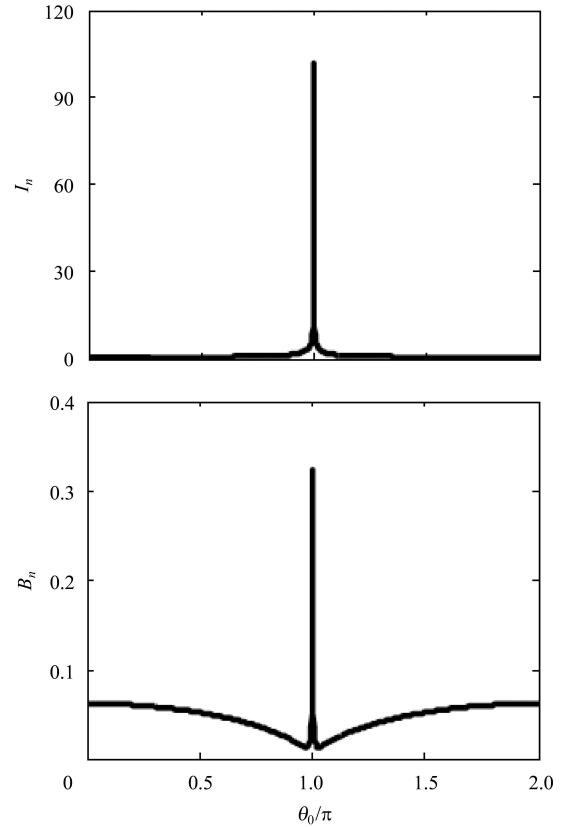

Fig. 2. The analytical estimate of the local current factor and local bunching factor at the modulator exit.

Since large energy modulation far beyond FEL pierce parameters [2] is introduced in the modulator, there is no exponential growth in the radiator. Then, for the case of a short radiator discussed here, longitudinal dynamic of the electrons is mainly determined by the undulator magnetic field, and the effects due to the radiation can be neglected. Thus, in the radiator the radiation caused by the coherent enhancement process is

$$a_{s2}(\theta_0, N_2) = a_{s2}\left(\theta_0 - \frac{2\pi}{n}, N_2 - 1\right) + \frac{r_e a_{u2} \lambda_{u2} \lambda_s I_0 [JJ]_2}{n\gamma_0 e c \Sigma} D_n(\theta_0, N_2), \quad (11)$$

where a_{s2} and a_{u2} are the dimensionless amplitude of the radiation field and the magnetic field of the radiator, respectively; r_e is the classical electron radius; λ_{u2} is the period length of the radiator; $[JJ]_2$ is the polarization modification factor for a linearly polarized planar undulator; I_0 is the initial uniform beam

current; Σ is the transverse beam area; c is the speed of light in vacuum and D_n is the local driving factor leading to the radiation, which is defined as:

$$D_n(\theta_0, N_2) = I_n(\theta_0, N_2)B_n(\theta_0, N_2). \qquad (12)$$

Using Eq. (11), one can analytically calculate the time structure and spectrum of the ultra-high order harmonic generation. However, Eq. (11) is too complicated for analytical optimization and qualitative discussion. In the following, we present a first approximation result. As shown in Fig. 2, the local current factor and the local bunching factor can be treated roughly as the δ function at the entrance of the radiator, thus

$$D_n(\theta_0, N_2) \approx D_n(\pi, N_2)\delta(\theta_0 - \pi). \qquad (13)$$

If the electron bunch in one seed wavelength radiates as a point charge, and accumulation of coherent harmonic generation will be absent in the short radiator. Thus, the radiation is determined by the local driving factor of the electron beam in the radiator:

$$P_{s2}(\theta_0, N_2) \propto n^2 a_n^2(\theta_0, N_2) \propto D_n^2(\pi, N_s) \qquad (14)$$

N_s is the radiator position where the radiation $a_n(\theta_0, N_2)$ is emitted. This obeys the law of causation, thus

$$0 < N_s = N_2 - \frac{\theta_0 - \pi}{2\pi/n} < N_2 . \qquad (15)$$

To explore the ultra-high order harmonic generation, we study the optimal $D_n(\pi)$ at the entrance of the radiator. The analytical dependence of the local current factor, the local bunching factor and the local driving factor on the frequency up-conversion factor is plotted in Fig. 3. When $n < 10^3$, the local driving factor increases for the sake of the enhancement of the local beam current. After that, the local driving factor decreases quickly due to the reduction in the local bunching factor. The driving factor is in the same order for $n = 10^4$ and $n=1$. This means that, when passing one radiator period, the peak radiation power of $n = 10^4$ is similar to that of $n=1$. However, one should notice that the average power of $n = 10^4$ is much less than that of $n=1$ for the micro-structure over the distance λ_s, and there is no coherent enhancement after passing more radiator periods for ultra-high order harmonic generation, as explained above.
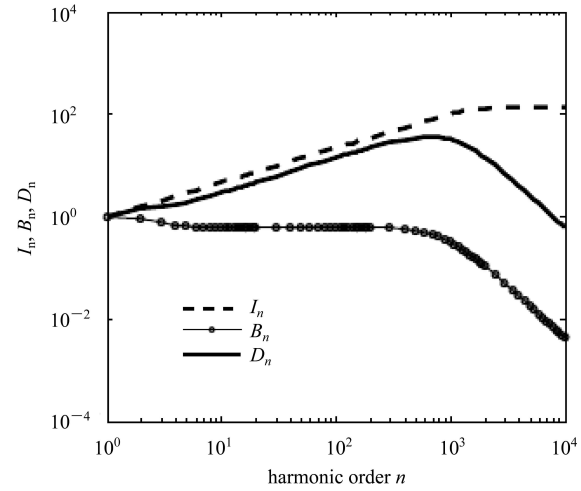

Fig. 3. Variation of the local current factor, the local bunching factor and the local driving factor at $\theta_0 = \pi$ with the increasing of the frequency up-conversion factor.

4　Soft X-ray example

To be specific, in this section we consider a soft X-ray example where $n = 1000$. Here we use a state-of-the-art electron beam with a peak current of 4 kA, energy of 4 GeV, relative energy spread of 1×10^{-5}, small emittance of 1 μm·rad and beam radius of 50 μm. An 800 nm seed pulse with 108 GW peak power, 0.7 mm laser waist and longitudinal uniform profile of 200 fs pulse length is injected into a 20-period modulator. The main parameters are summarized in Table 1. The 0.8 nm output soft X-ray radiation is investigated below.

Table 1.　Main parameters of soft X-ray example.

parameters	value
seed laser wavelength/nm	800
seed laser power/GW	108
seed laser duration/fs	200
seed laser waist/mm	0.7
electron beam energy/GeV	4
peak current/kA	4
normalized emittance/(μm·rad)	1
local energy spread/keV	40
modulator period length/m	0.20
modulator period number	20
radiator period length/mm	50
radiator period number	1–100
radiator resonant wavelength/nm	0.8

The beam dynamics in the modulator are simulated by FEL code GENESIS1.3 [23], which has been widely used in the simulations of many FEL projects

around the world. 10^6 macro-particles are applied to represent the electrons over the distance λ_s. The longitudinal phase space of the electron beam shown in Fig. 4. After the modulator, the initially uniform electron distribution becomes strongly disturbed, and a significant fraction of the beam is compressed into a sheet that is thinner than the radiator resonant wavelength. Thus the ultra-high order harmonic bunching builds up.
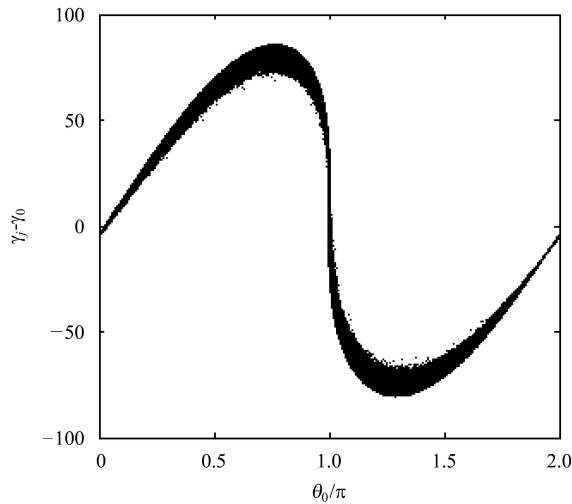

Fig. 4. The longitudinal phase space of the electron beam at the modulator exit from 3D simulation.

To compare the analytical estimate with 3D simulation, we first consider the optimal energy modulation induced in the modulator. In the analytical model, the optimal energy modulation is $\Delta\gamma$=62.5, while in the simulation the optimal seed laser produces an energy modulation of $\Delta\gamma$=85.7. Then we plot the local current factor and local bunching factor in Fig. 5. At the position of $\theta_0 = \pi$, the local current factor is about 96 and the local bunching factor is 0.28. Considering that crude approximations have been taken in the analytical estimate, there is good agreement between the analytical estimate and numerical simulation. Several comparisons for different cases have been carried out. The agreement is generally good within a factor of 2.

For ultra-high order harmonic generation, in current state-of-the-art numerical modeling, the evolution of radiator radiation is on the basis of the average over one seed laser wavelength. When the harmonic number is up to 1000, to our knowledge, the radiator radiations with micro-structure cannot be appropriately simulated by publically available 3D code. To extend the computation, the electron beam distribution generated by GENESIS1.3 is posterior processed

after each integral step, and the modified particle distribution is implanted to the next standard run of GENESIS1.3. With such a loop, more realistic 3D numerical modeling is developed [24].
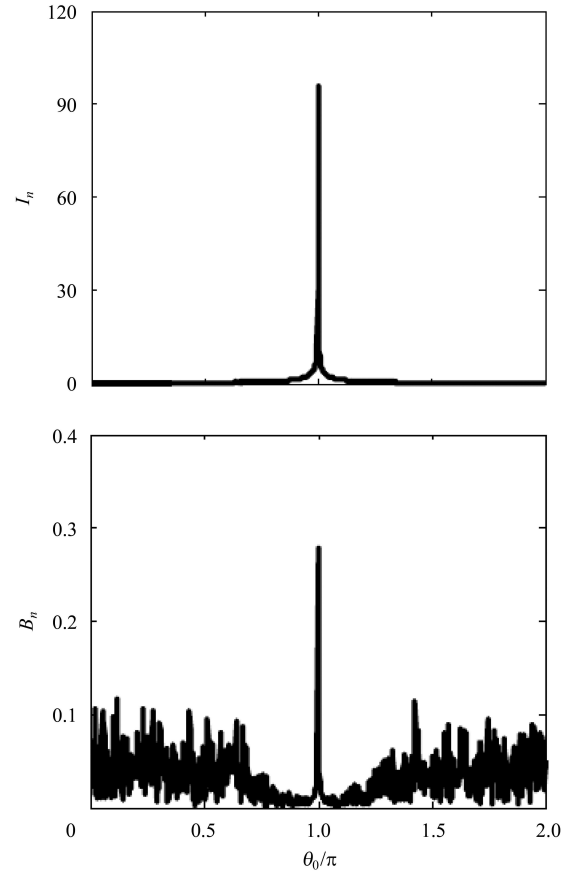

Fig. 5. The local current factor and local bunching factor at the modulator exit from 3D simulation.
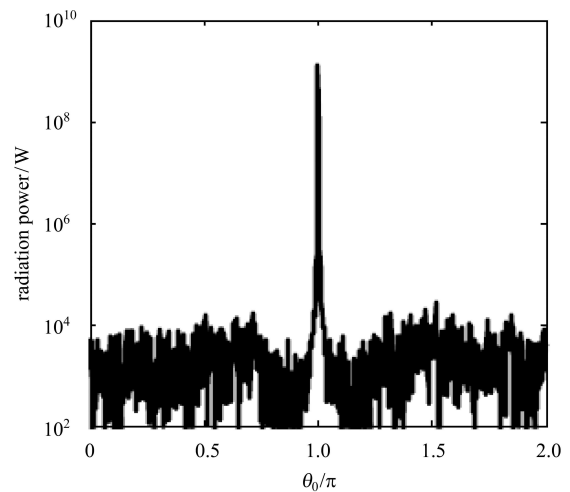

Fig. 6. The simulated micro-structure of the radiation after passing 1 radiator period.

According to the simulation results, a set of attosecond trains are observed after passing one radiator period. The distance between two trains is one seed laser wavelength. In our case, it is 800 nm (i.e. 2.7 femtosecond). One of the radiation trains is shown in Fig. 6. The pulse duration is 3.3 attosecond. This is slightly larger than the oscillation duration of 0.8 nm radiation. In more detail, the radiation power is about 1.32 GW, corresponding to an electric field of 10 GV/m on the radiator axis. In contrast, the radiation power from shot noise is about 10 kW. The ratio of signal to noise is about 10^5. This is highly consistent with the analytical estimate.

5   Stability and coherence

The main jitter source for ultra-high order harmonic generation is the power fluctuation of the high intensity seed laser. The fluctuation in the seed laser power can be well controlled below 0.5%, which leads to a 0.25% jitter in the energy modulation. These jitters can be compensated by the dispersion of the radiator. As variation of the local driving factor at $\theta_0 = \pi$ in the radiator given in Fig. 7, where $n = 1000$, the local driving factor has a stable performance within 100 radiator periods. Therefore, according to Eq. (14), relatively stable radiation may be expected.
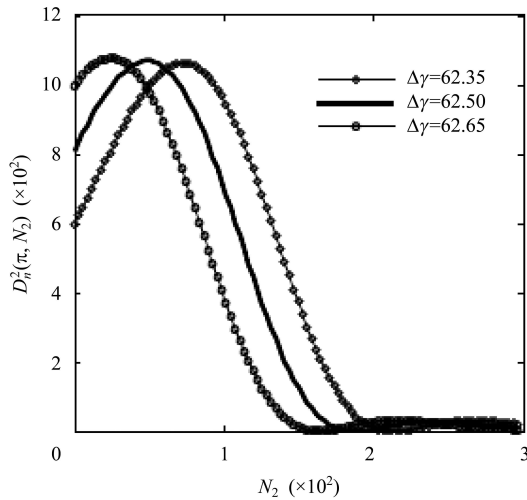

Fig. 7.   Variation of the local driving factor of the electron beam at $\theta_0 = \pi$ in the radiator, The results are analytically from Eq. (12).

Figure 7 also indicates that, due to slippage effects, the output pulse duration can be adjusted by changing the period number of the radiator. In the soft X-ray example, where the wavelength is 0.8 nm, with the increasing number of radiator periods from 1

to 100, the output pulse duration increases from 2.7 to 270 attoseconds. In order to support our conclusion, we plot the radiation power at $N_2 = 100$ in Fig. 8. The main pulse duration is about 270 attoseconds, which is 100 times the oscillation duration of 0.8 nm. In more detail, the main radiation peak looks like a saddle. This is because the local driving factor is not really a δ function. The radiated fields between the two peaks are the averaged result of the local driving factor around $\theta_0 = \pi$. If we analytically calculate the radiation power by the accurate Eq. (11), a similar saddle will be observed.
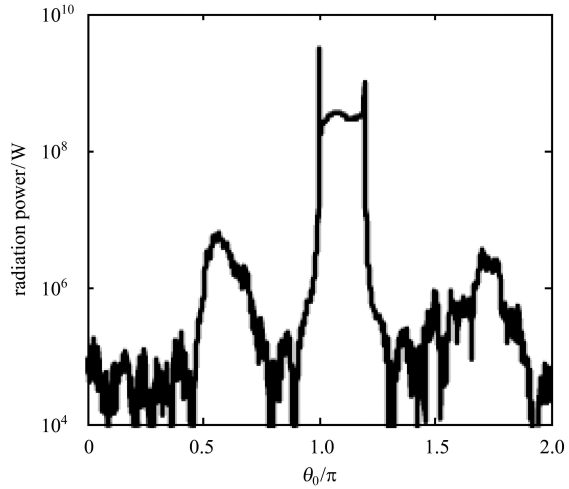

Fig. 8.   The simulated micro-structure of the radiation after passing 100 radiator periods.

Since the radiation is a set of finite trains with a periodic duration of 800 nm, its spectrum is expected to be a number of spectral lines appearing at the harmonics of the seed laser. Fig. 9(a) shows the spectrum of the photons radiated after 100 radiator periods. The envelope of those solid lines is determined by the pulse duration of coherent harmonic generation, which performs as the spontaneous emission spectrum of a single electron. The subtle structure of one spectral line is illustrated in Fig. 9(b), which is a characteristic feature of the seed laser assisted harmonic production. The bandwidth of the 0.8 nm radiation is about 3×10^{-5}. This is commensurate with the bandwidth of an X-ray FEL.

Finally, we consider the transverse distribution of the radiation. As plotted in Fig. 10, the radiation size is 51 μm, and the diffraction angle of the radiation is 15 μrad. Thus, the emittance of the 0.8 nm radiation is about 0.77 nm, which is close to the diffraction limit of a Gaussian beam. Thus, the ultra-high order harmonic generation shows a fully transverse coherence.
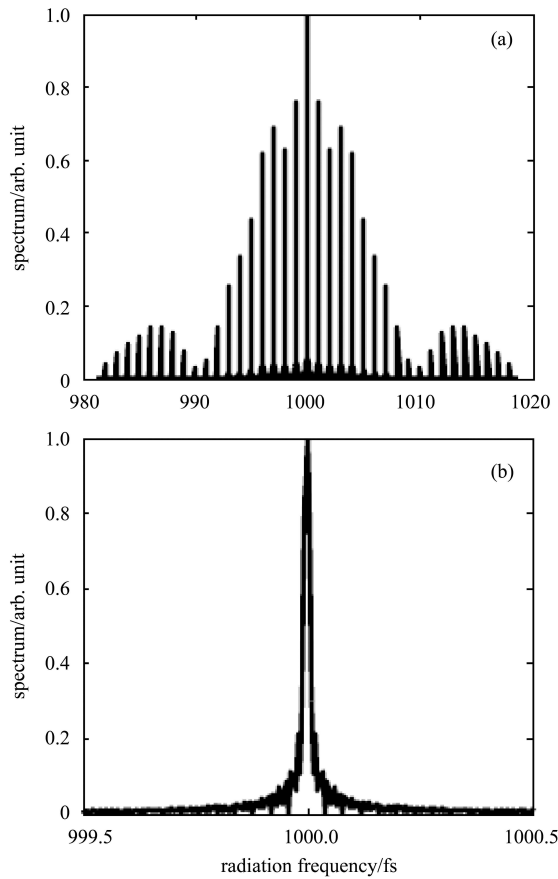
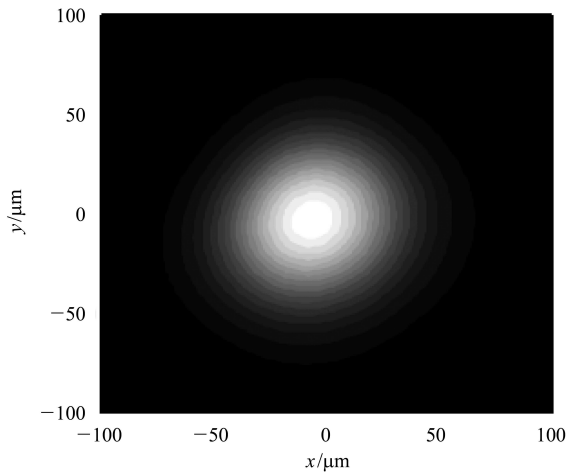Fig. 9. The simulated spectrum after passing 100 radiator periods.

Fig. 10. The simulated transverse radiation distribution.

6   Conclusions

Using two undulators and an external seed laser, great potential for ultra-high order harmonic generation via FEL mechanism is demonstrated. In such a system, attosecond trains can be produced from the deep ultraviolet to the hard X-ray spectral regions. In this paper, a soft X-ray example is presented. We use the relativistic electron bunch with the typical quality as in the SASE scheme, and a seed laser with a wavelength of 800 nm and a peak power of 108 GW. The 0.8 nm radiation trains with peak power of GW scale are generated. The output pulse duration is proportional to the radiator period number, and the output radiation has a perfect tuning ability between the discrete harmonics of the seed frequency.

The attosecond structure of ultra-high order harmonic generation can be further amplified by the FEL scheme [25, 26]. Compared with high order harmonic generation (HHG) in rare gases [27–30], the ultra-high order harmonic generation via the FEL mechanism is mainly determined by the "cool" electron beam. Thus, much better coherence and higher frequency up-conversion efficiency may be observed. In this discussion, we have assumed that a 200 femtosecond seed pulse with a longitudinal uniform profile and a set of attosecond trains are emitted. The continuous progress in laser technology makes possible the generation of ultra-short and high intensity pulses [31, 32]. If we use a sub-10 fs seed pulse with a peak power on the terawatt scale, together with the slippage effects in the modulator and the right parameters, single attosecond X-ray pulses can also be emitted in the radiator.

It is worth stressing that the results are preliminary. In reality, a chicane or dogleg is needed to separate the electron beam from the seed laser. Then a strong coherent synchrotron radiation effect may reduce the quality of the electron beam entering the radiator. What's more, the space charge effect is not included in this study. There is still room for improvement, which will be addressed our subsequent reports.

References

1 Debenev Y S, Kondratenko A M, Saldin E L. Nucl. Instrum. Methods A, 1982, **193**: 415
2 Bonifacio R, Pellegrini C, Narducci L M. Opt. Commun., 1984, **50**: 373
3 YU L H. Phys. Rev. A., 1991, **44**: 5178
4 WU J H, YU L H. Nucl. Instrum. Methods A, 2001, **475**: 104
5 Goloviznin V V, Amersfoort P W. Phys. Rev. E, 1997, **55**: 6002
6 YU L H, Babzien M, Ben-Zvi I et al. Science, 2000, **289**: 932
7 YU L H, DiMauro L, Doyuran A et al. Phys. Rev. Lett., 2003, **91**: 074801
8 Saldin E L, Schneidmiller E A, Yurkov M Y. Opt. Commun., 2002, **202**: 169
9 Allaria E, Ninno G D. Phys. Rev. Lett., 2007, **99**: 014801
10 JIA Q K. Appl. Phys. Lett., 2008, **93**: 141102
11 Stupakov G. Phys. Rev. Lett., 2009, **102**: 074801
12 Akre R, Dowell D, Emma P et al. Phys. Rev. ST Accel. Beams., 2008, **11**: 030703
13 HUANG Z, Borland M, Emma P et al. Phys. Rev. ST Accel. Beams., 2004, **7**: 074401
14 YU L H, WU J H. Nucl. Instrum. Methods A, 2002, **483**: 493
15 DING Y, Brachmann A, Decker F J et al. Phys. Rev. Lett., 2009, **102**: 254801
16 Rosenzweig J B, Alesini D, Andonian G et al. Nucl. Instrum. Methods A, 2008, **593**: 39
17 Zholents A, Fawley W M. Phys. Rev. Lett., 2004, **92**: 224801
18 Saldin E L, Schneidmiller E A, Yurkov M V. Opt. Commun., 2004, **237**: 153.
19 Emma P, Bane K, Cornacchia M. Phys. Rev. Lett., 2004, **92**: 074801
20 Zholents A. Phys. Rev. ST Accel. Beams., 2005, **8**: 040701
21 JIA Q K. Phys. Rev. ST Accel. Beams., 2005, **8**: 060701
22 Sears M S, Colby E, Ischebeck R et al. Phys. Rev. ST Accel. Beams., 2008, **11**: 061301
23 Reiche S. Nucl. Instrum. Methods A, 1999, **429**: 243
24 DENG H X, DAI Z M. Nucl. Sci. Tech., 2010, **21**: 321
25 Garzella D, Hara T, Carre B et al. Nucl. Instrum. Methods A, 2004, **528**: 502
26 Thompsom N R, McNeil B W J. Phys. Rev. Lett., 2008, **100**: 203901
27 Macklin J J, Kmetec J D, Gordon C L. Phys. Rev. Lett., 1993, **70**: 766
28 Lewenstein M, Balcou P et al. Phys. Rev. A, 1994, **49**: 2117
29 Bartels R A, Paul A, Green H et al. Science, 2002, **297**: 376
30 Popmintchev T, Chen M C, Cohen O et al. Opt. Lett., 2008, **33**: 2128
31 Brabec T, Krausz F. Rev. Mod. Phys., 2000, **72**: 545
32 Seres J, Müller A, Seres E. Optics Letters, 2003, **28**: 1832